TURBULENCE PHYSICS OF COMPRESSIBLE BOUNDARY LAYERS

Maher Lagha, John Kim, Jeff Eldredge & Xiaolin Zhong
Mechanical and Aerospace Department
University of California, Los Angeles
420 Westwood Plaza, Los Angeles CA 90095-1597, USA
Email: maher.lagha@gmail.com

ABSTRACT

Compressible turbulent boundary layers with free-stream Mach number ranging from 2.5 up to 20 are analyzed by means of direct numerical simulation of the Navier–Stokes equations. The fluid is assumed to be an ideal gas with constant specific heats. The simulation generates its inflow condition using a rescaling-recycling method. The main objective is to study effects of Mach number on turbulence statistics and near-wall turbulence structures. The present study shows that the main turbulence statistics can be correctly described as variable-density extensions of incompressible results. The study also shows that turbulence in the near-wall region can be sustained without turbulence in the outer region, proving the existence of a local cycle within the near-wall region. Physics of near-wall turbulence is investigated in a simplified model flow, where the coherent part of turbulence is separated from the rest by a Galerkin projection. It is shown that the near-wall region is populated by crescent-shaped vortical structures, which are associated with regions with positive Reynolds stress production.

1 Introduction

The design of supersonic and hypersonic vehicles depends critically on the accurate prediction of turbulent flow characteristics in high Mach number boundary layers. Basic knowledge and understanding of both aerodynamic and thermodynamic phenomena are the prerequisites in order to use design tools effectively.

The understanding of complex flow phenomena can best be obtained through a coordinated study involving both computational and theoretical analyses. Relatively few numerical simulations of a turbulent supersonic boundary layer are available in the literature. Most of these studies were primarily focused on the effects of compressibility on turbulence statistics at relatively low Mach numbers (≤ 5). Very few studies aimed at improving the understanding of the fundamental physics of supersonic boundary layers have been conducted.

It is known that, for supersonic flows with moderate Mach numbers, the direct effects of compressibility on wall turbulence at zero pressure gradient are small, the most notable differences being due to the variation of the thermodynamic properties across the layer. This is known as the Morkovin hypothesis. All available experimental data (see Smits & Dussauge (2006) and references therein) confirm that supersonic boundary layers at zero pressure gradient exhibit close similarities to incompressible ones, and that the main turbulence statistics can be correctly predicted as variable-density extensions of incompressible results.

These similarities have been confirmed by recent direct numerical simulations, which include the extended temporal simulation of Maeder *et al.* (M_∞=2.5) (2001), the quasi-periodic simulation of Guarini *et al.* (M_∞=2.5) (2000), and the fully spatial simulations of Martin (M_∞ up to 8) (2004) and Pirozzoli *et al.* (M_∞=2.25) (2004). These studies have further confirmed the validity of the Van Driest transformation for the mean velocity profile and that the distributions of the density-scaled root-mean-square fluctuations of the velocity and vorticity closely follow the universal distribution found in the incompressible case.

The fundamental physics of turbulence in high Mach number boundary layers are poorly understood. Experiments are costly and difficult to conduct, and very few numerical simulations at high Mach numbers have been reported (see references). There are numerous challenges in order to perform numerical simulation of a high Mach number turbulent flow.

We have developed a hybrid numerical scheme coupling a fifth-order weighted essentially non-oscillatory (WENO) scheme for high gradient regions and an upwind fifth-order finite difference scheme for computing turbulence in the smooth region. This hybrid scheme is computationally less expensive and less dissipative than the WENO scheme. The viscous fluxes are approximated using a sixth-order finite-difference scheme, and the time integration is performed by means of a classical four-stage fourth-order explicit Runge–Kutta scheme. This numerical scheme was validated against various compressible flows, and the interested reader is referred to Lagha *et. al* (2009) for further details.

2 Inflow boundary conditions

The generation of a turbulent inflow for the numerical simulation of a boundary layer is in itself an issue, owing to the difficulty of obtaining a physical turbulent flow at a reasonable computational cost. Different approaches, including

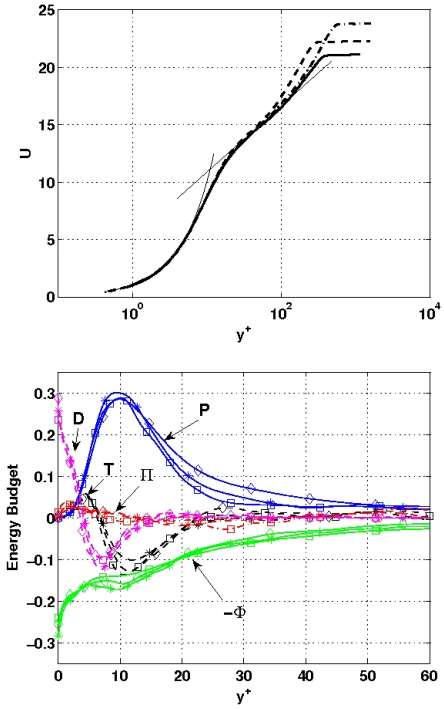

Figure 1. Top: Mean velocity profile. Bottom: Energy budget. M_∞=2.5 ($*$), 10 ($\diamond$) and 20 (square).

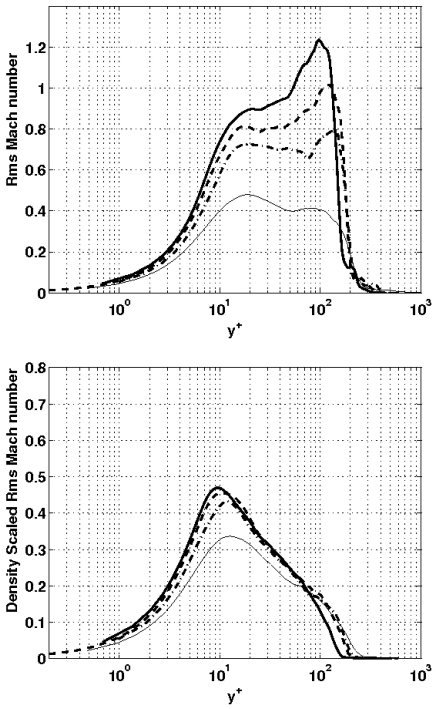

Figure 2. Profiles of M' for M_∞=5 (thin solid-line), M_∞=10 (-.-.-.-), M_∞=15 (- - - -) and M_∞=20 (—). Without (top) and with (bottom) mean density scaling.

temporal boundary layer (TDNS), extended TDNS (ETDNS) and spatial boundary layer (SDNS), have been developed. In the latter case, the simulation generates its own inflow conditions by rescaling the flowfield at a downstream station $x_{\rm re}$ and prescribing it at the inlet. This method was applied by Lund *et al.* (1998) and Ferrante & Elghobashi (2004) to incompressible boundary layer, and its extension to the compressible flow was developed by Urbin & Knight (1998). We have improved this technique and made it easy-to-implement. The details of the method are given in Lagha *et. al* (2011). The final Reynolds number R_τ based on the friction velocity is also easy to control. For all the simulations, the streamwise L_x, wall-normal L_y and spanwise L_z extents of the domain are $L_x \times L_y \times L_z = 14\delta_{99} \times 5\delta_{99} \times 2\delta_{99}$. The recycling station is located at $x_{\rm re} = x_{\rm in} + 8\delta_{99}$. Two sponge regions are added near the outlet (starting at $x = x_{\rm in} + 13\delta_{99}$) and the top of the domain (starting at $y = 4\delta_{99}$) to prevent artificial reflections from the boundaries (see Xu & Martin (2004), Lagha *et al.* (2009)). Periodic boundary condition is used in the spanwise direction. In all cases, the number of points in the streamwise, wall-normal and spanwise direction is $N_x \times N_y \times N_z = 512 \times 128 \times 256$. The grid resolutions in wall units are $\Delta_x^+ \times \Delta_y^+ \times \Delta_z^+ \approx 8\times\ 0.3\times\ 3$. A hyperbolic stretching is used in the y-direction and at the boundary layer edge, $\Delta_y^+ \approx 11$. Higher resolutions (up to $1024 \times 180 \times 512$) were used to validate the accuracy of the simulations.

3 Turbulence statistics

To validate the present simulation, the computed mean velocity, Reynolds stress and the root-mean-square (rms) of the velocity and vorticity components were compared with the adiabatic results of Guarini *et al.* at M_∞=2.5 and showed a good agreement. Simulations with higher Mach numbers M_∞=10 and M_∞=20 have also been performed. The distribution of the van Driest-transformed mean streamwise velocity, expected to satisfy the incompressible log law, is shown in Fig. 1.

The distributions of the density-scaled Reynolds-stress components, $\sqrt{\overline{\rho}/\rho_{\rm w}}\sqrt{u_i'^2}/u_\tau$, collapse with the incompressible results. A similar observation holds for the vorticity fluctuations and the energy budget. The fluctuating Mach number M' is found to be sensitive to M_∞. For low M_∞ (≤ 5), its maximum is near the wall and for higher M_∞, M' starts to build a second maximum away from the wall, as seen in Fig. 2.

In order to differentiate between a true compressibility effect and a variable property effect, we have studied the origin of this behavior. We have shown that the apparent increase in the magnitude of the fluctuating Mach number with increasing M_∞ is a variable-property effect. Using the mean density to scale the fluctuating Mach number collapses results for different M_∞, as shown in Fig. 2. For futher discussions on the effects of Mach number on turbulence statistics, the interested reader is referred to Lagha *et al.* (2011).

4 Turbulence structures

In a numerical study of channel flow, Coleman *et al.* (1995) observed an increase with the Mach number of the streamwise coherence of the near-wall streaks. They showed

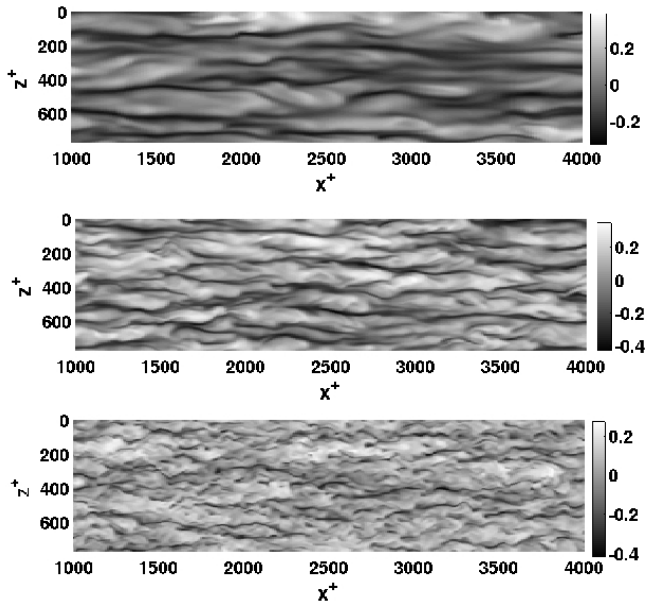

Figure 3. Streamwise velocity perturbations. Top to bottom: $\frac{T_w}{T_\infty}$=1, $\frac{T_w}{T_\infty}$=2.14, $\frac{T_w}{T_\infty}$=11.6.

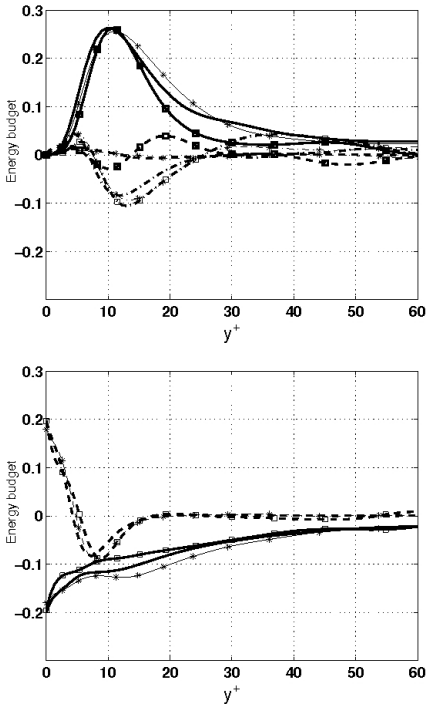

Figure 4. Kinetic energy budget. Top: Production P (—), Transport T (-.-.), Pressure term Π (- - -). Bottom: viscous diffusion D (- - -) and viscous dissipation $-\Phi$ (—). Line with no symbols: unfilterd flow. Line with stars: flow above $y^+ \geq 60$ is filtered. Line with squares: flow after Galerkin projection, where $v'_{\rm inc}$ was removed.

that this modification of turbulence structure represents a confirmation of, and not an exception to, the Morkovin hypothesis, which postulates that at supersonic Mach numbers only mean property variations are important and not the thermodynamic fluctuations. To further study the effect of the Mach number on the near-wall structures, we have performed three isothermal simulations, where the wall-temperature was varied from $\frac{T_w}{T_\infty}$=1 (cold wall) to $\frac{T_w}{T_\infty}$= 2.14 ($\approx \frac{T_{\rm adiab}}{T_\infty}$) and $\frac{T_w}{T_\infty}$=11.6 (hot wall). The free-stream Mach number was fixed at M_∞=2.5. In accordance to the results of Coleman *et al.* and of Duan *et al.*, the streaks streamwise coherence increased when the wall was cooled, as shown in Fig. 3. They also became shorter when the wall was heated. We have also found that the streaks are not modified when the gradients of mean properties are zero, namely for an adiabatic wall. In this case, their typical spanwise spacing of 100 wall units is still valid, even at M_∞=20.

5 Near-wall dynamics

Direct numerical simulations provide detailed flow field with which we can investigate relevant flow physics. However, it produces a huge amount of temporal three-dimensional data. Its direct analysis remains elusive. Many attempts have been made recently to reduce the complexity of flow dynamics in the near-wall region, where most of the energy production occurs. Since most of the main statistics for the higher Mach numbers are similar to these of the subsonic case, it is expected that the essential mechanisms of turbulence dynamics would be the same for different Mach numbers. In this paper, we therefore consider the results obtained using the flow fields at $M_\infty = 2.5$.

The complexity of the dynamics in the near-wall region ($y^+ \leq 60$) can be reduced by eliminating the interactions with the outer region. This is achieved by damping all the perturbations for $y^+ \geq 60$. After a short transient during which all the fluctuations above $y^+ = 60$ are mostly damped, the turbulent flow in the inner region survives and settles to $R_\tau \approx 324$, close to the unfiltered $R_\tau \approx 350$.

The rms of the velocity fluctuations as well as the kinetic energy budget are very close to the original results of the unfiltered flow as shown in Fig.4, thus demonstrating that an outer flow is not needed for the maintenance of near-wall turbulence, or even for defining its quantitative properties. This illustrates the existence of a local self-sustaining process for the turbulence in the inner region in compressible turbulent boundary layers. This is in agreement with the results of Jimenez & Pinelli (1999) for the incompressible case.

In order to gain further insight into near-wall turbulence physics, we have to isolate the coherent part of turbulence from the background flutuations. Separating the coherent vortices from the background turbulence provides a clear picture of the dynamics of the streamwise vortices populating the near-wall region. The equations of motion are integrated as usual, but at each time step, v' is decomposed into a coherent part, representing streamwise vortices filling the entire gap between $y^+ = 0$ and $y^+ = 60$, and an incoherent part representing the background turbulence: $v' = v'_{\rm vor} + v'_{\rm inc}$. Then, $v'_{\rm inc}$ is removed. A Galerkin projection is used to compute

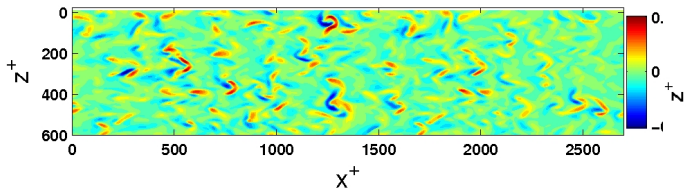

Figure 5. Spatial distribution of the wall-normal velocity at $y^+ \approx 15$ in a (x',z')-plane.

the coherent part. The rms quantities of this filtered flow are close to these of the original simulation, as shown in Fig.4. Fig. 5 shows a typical velocity field plot of the instantaneous velocity fluctuation v' at $y^+ = 20$. In this figure the flow is from left to right. The pattern which is mostly recognizable has a crescent shape. Each one corresponds to two counter-rotating vortices, as revealed by the cross-stream section $(y\text{-}z)$ of the flow field (v',w') in Fig. 6. Positive patches of v' corresponds to negative patches of u', and vice versa. This $u'v'$-anticorrelation, which gives positive Reynolds shear stress $-u'v'$, is associated with the so-called lift-up mechanism.

The induced positive and negative u' fluctuations via this mechanism correspond, respectively, to high and low speed streaks. These streaks span the entire near-wall region up to $y^+ \approx 60$ (Fig. 6).

The crescent vortices and velocity fields in both the (x,z)- and (z,y)-planes shown in Fig. 6 come from an individual snapshot, but the patterns are representative of those found across the whole field at different times. These flow structures are significant to the turbulent flow dynamics in the near-wall region, since they occur frequently in the flow and are associated with most positive Reynolds shear stress events. Both kinds of crescent vortices and their relation to one another are discussed in detail in Lagha *et al.* (2011).

The structure of the flow around these regions of turbulent kinetic energy production is very similar to that obtained by Johansson *et al.* (1991) in channel flow using the VISA/VITA technique. For example, the structure of the velocity component u' is very similar to the one given in Figures 5 and 6 in Johansson *et al.* (1991), highlighting a negative $\partial_x u'$ with a stagnation point $u' \approx 0$. Around this point, the v' observed in Fig. 7 has similar topology as in Figures 5 and 6 in Johansson *et al.* (1991), with $\partial_x v' \geq 0$. This positive gradient of v' is the signature of a spanwise vortex with positive ω_z', which constitutes the head of crescent vortices. Note that the quadrupolar flow (u',w') is not symmetrical around the stagnation point, as is the case in Johansson *et al.* (1991). This is due to the fact that the symmetry with respect to x in the channel flow simulation is absent in the boundary layer flow.

6 Conclusion and Future work

To improve our understanding of the fundamental physics of supersonic boundary layers, we have performed a parametric study varying the free-stream Mach number and the wall-temperature. The turbulence statistics collapse into their incompressible counterparts when rescaled using the wall quantities.

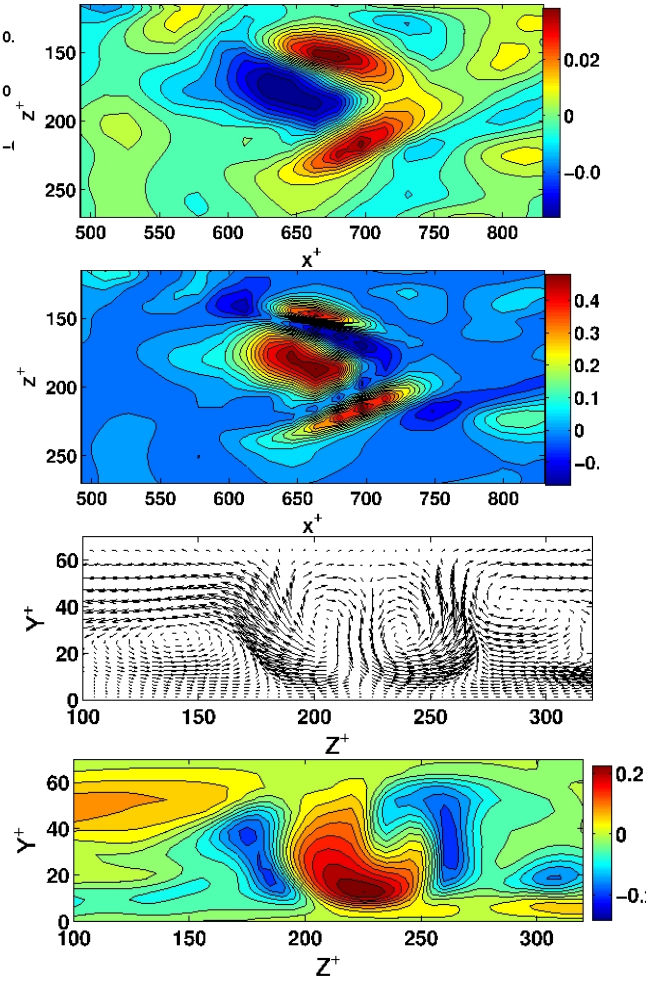

Figure 6. Features of a typical crescent vortex. Top to bottom: 1) Spatial distribution of v' at $y^+ \approx 15$; 2) Spatial distribution of $-u'v'$ at $y^+ \approx 15$; 3) Cross-stream distribution of (v',w') at $x^+ \approx 680$; 4) Cross-stream distribution of u'.

We have demonstrated that crescent-shaped vortical structures, which contain both signs of streamwise vorticity, populate the near-wall region. We have analyzed the flow around these vortical structures, and have shown that it is similar to the internal shear layer iden- tified by other techniques in incompressible flows. We have also provided a physical interpretation of the crescent-shaped vortical structure: a spanwise vortex with positive ω_z', surrounded by a quadrupolar flow having a stagnation point $u' \approx 0$, and stretched by positive $\partial_z w'$ in the z-direction. This crescent vortical structure forms the basis of our proposed conceptual model, in which streamwise vortices are generated through tilting of positive ω_z' by the streaks $(\omega_z' \partial_z u')$ and then stretched in the x-direction $(\omega_x' \partial_x u')$. Through the lift-up mechanism, these streamwise vortices create streaks.

Although we have used a compressible boundary layer in this study, considering the results reported in Lagha *et al.* and some results presented here for different Mach numbers, the essential elements of the crescent-shaped vortical structures discussed in the present paper apply to both compressible and

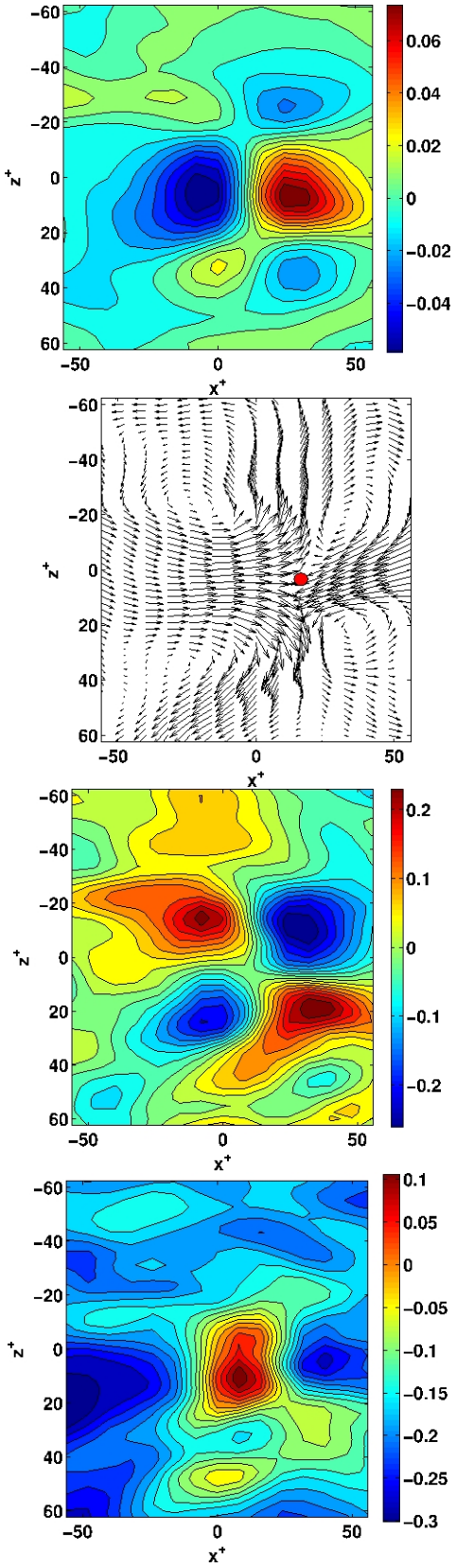

Figure 7. Statistics of the crescent vortices. Top to Bottom: v', flow field (u', w') in (x^+, z^+)-plane (the dot marks a stagnation point), streamwise $\omega_x' \nu_w / u_\tau^2$ and spanwise $\omega_z' \nu_w / u_\tau^2$ vorticity components.

incompressible boundary layers.

REFERENCES

A. J. Smits & J. P. Dussauge, "Turbulent Shear Layers in Supersonic Flow." American Institute of Physics, New York.

T. Maeder, N. A. Adams & L. Kleiser, "Direct simulation of turbulent supersonic boundary layers by an extended temporal approach." J. Fluid Mech. **429**, (2001) 187–216.

S. E. Guarini, R. D. Moser, K. Shariff & A. Wray, "Direct numerical simulation of a supersonic boundary layer at Mach 2.5." J. Fluid Mech. **414**, (2000) 1–33.

M. P. Martin, "DNS of hypersonic turbulent boundary layers." AIAA Paper 2004–2337. S. Pirozzoli, F. Grasso & T. B. Gatski, "Direct numerical simulation and analysis of a spatially evolving supersonic turbulent boundary layer at M=2.25." Phys. Fluids **16** (3), 530–545.

M. Lagha, X. Zhong, J. Eldredge & J. Kim, "A Hybrid WENO scheme for the simulation of shock wave-boundary layer interaction." AIAA Paper 2009–1136.

M. Lagha, J. Kim, J. D. Eldredge, & X. Zhong, "A numerical study of compressible turbulent boundary layers." Phys. Fluids **23** (1), 015106, (2011).

M. Lagha, J. Kim, J. D. Eldredge, & X. Zhong, "Near-wall dynamics of compressible boundary layers." Submitted to Phys. Fluids.

G. N. Coleman, J. Kim & R. D. Moser, "A numerical study of turbulent supersonic isothermal-wall channel flow." J. Fluid Mech. **305** (1995) 159–183

M. J. Ringuette, M. Wu & M. P. Martin, "Coherent structures in direct numerical simulation of turbulent boundary layers at Mach 3." J. Fluid Mech. **594**, 59–69, (2008).

L. Duan, I. Beekman & M. P. Martin, "Direct numerical simulation of hypersonic turbulent boundary layers. Part 2. Effect of wall temperature." J. Fluid Mech. **655** (2010), 419–445.

L. Duan, I. Beekman & M. P. Martin, "Direct numerical simulation of hypersonic turbulent boundary layers. Part 3. Effect of Mach number" J. Fluid Mech. **67x** (2011), 1–23.

T. Lund, X. Wu & K. Squires, "Generation of turbulent inflow data for spatially developing boundary layer." J. Comp. Phy. **140**, (2), (1998), 233–258.

G. Urbin & D. Knight, "Large-Eddy Simulation of a supersonic boundary layer using an unstructured grid." AIAA J. Vol **39**, (7), (2001), 1288–1295.

A. Ferrante & S. E. Elghobashi, "A robust method for generating inflow conditions for direct simulations of spatially-developing turbulent boundary layers." J. Comput. Phys. **198**, (2004) 372.

J. Jimenez & A. Pinelli "The autonomous cycle of near-wall turbulence." J. Fluid. Mech. **389** 335–359, (1999).

A. V. Johansson, P. H. Alfredsson, & J. Kim, "Evolution and dynamics of shear-layer structures in near-wall turbulence." J. Fluid Mech. **224**, 579–599, (1991).